Two-Dimensional Method for Calculating Separated Flow in a Centrifugal Impeller

D. P. STURGE

N. A CUMPSTY

Department of Engineering,
University of Cambridge,
Cambridge, England

A method of calculating a two-dimensional incompressible and inviscid flow within a centrifugal impeller where the flow separates from the suction side has been developed. Based on experimental observation it has been assumed that mixing of the throughflow with the separated region is suppressed. After a description of the calculation method, which is rather unusual, some results are presented and the implications discussed. The possibility of extending the method to handle compressible flow is outlined.

1 Introduction

Many papers have been written on the numerical calculation of the flow patterns in centrifugal impellers. There are the famous papers of Stanitz [1, 2][1] from the fifties and more recently Katsanis [3] and Senoo and Nakase [4] have produced methods more suitable for digital computers. Despite this work, the flow in impellers is known to be very often separated; the first report of this was made by Fischer and Thoma [5] in 1932. Dean [6] has studied this aspect extensively and found that the separated region, or wake, may occupy as much as 70 percent of the passage area at exit. Moreover the interface between the main flow and the wake tends to behave like a low Reynolds number shear flow with very little mixing. This effect can be explained by the stabilizing effect of Coriolis forces on the shear layer described by Bradshaw [8] and has been beautifully demonstrated in the work at Stanford University [14, 15].

An example of a design calculation method incorporating division of the flow into a main throughflow region and a wake region is the one-dimensional method of Dean [7], in which the mean properties of the flow are treated separately.

The present two-dimensional calculation is an attempt to allow for this separation by means of a simplified mathematical model. The steady relative flow in an impeller passage is divided into two regions. The flow in the main region is regarded as inviscid and irrotational, while in the wake region there is no flow. The boundary between the two is treated as a free shear layer without mixing, which behaves rather like an air-water interface. The position of this boundary is defined by the condition that there is no change in static pressure across it, and that in the wake, because there is no flow, the reduced pressure ($p - \int \rho r\Omega^2 dr$) is constant.

In the throughflow region the equations expressing continuity and irrotationality must be solved numerically. The wake region affects the solution by determining the position of one of the boundaries. During the iterations, the position of the edge of the wake varies, and this leads to programming complexity. This problem can be avoided by inverting the equation for irrotationality (the continuity equation has been removed by using a stream-function ψ). The angular coordinate of the lines of constant ψ (streamlines) is then the dependent variable, with stream-function and meridional distance as the independent variables. The value of ψ is fixed at the edge of the wake.

The type of impeller considered is one with axial inlet and radial outlet, as shown in Fig. 1. Variations in flow properties normal to a mean flow surface are not taken into account, this mean flow surface being generated by rotation of a meridional line about the axis. Between inlet and outlet the shape of the mean flow surface, the height of the passage, and the number, thickness and shape of the blades are all arbitrary.

After describing the method, a few results for radial outlet and swept-back blades are shown. From these it is possible to draw some conclusions about the existing unseparated methods of calculation.

2 Idealization of the Flow

For the calculation the flow is regarded as inviscid, incom-

[1]Numbers in brackets designate References at end of paper.

Contributed by the Fluids Engineering Division of THE AMERICAN SOCIETY OF MECHANICAL ENGINEERS and presented at the Fluids Engineering Conference, Minneapolis, Minn., May 5-7, 1975. Manuscript received at ASME Headquarters January 20, 1975.

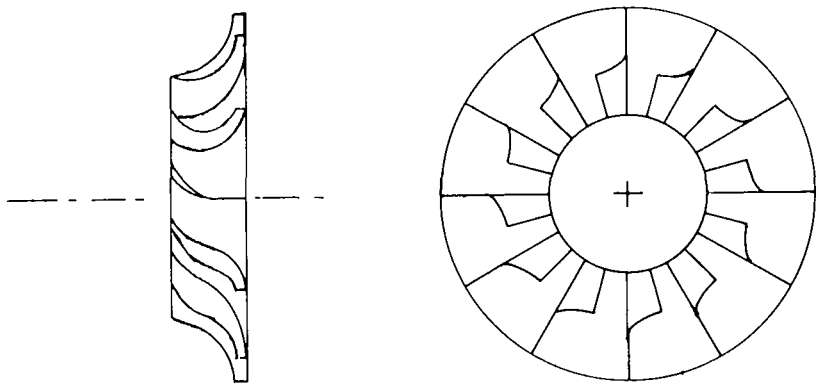

Fig. 1 Impeller with axial inlet and radial outlet

pressible and irrotational in the absolute frame of reference. It is also considered to be quasi-two-dimensional i.e., not varying across the passage in a direction normal to the mean flow surface defined previously. The validity of each of these assumptions is discussed in the following.

The inviscid approximation may be criticized for two reasons. Firstly, the flow is known to be turbulent over much of the passage as a result of boundary layer growth, the small passage height and the wakes of upstream guide vanes or intake supports; secondly considerable losses occur in the passage. Unfortunately, the alternatives are also considerably more complicated without being much more realistic, while an eddy viscosity with wall slip still does not fully model the flow and requires many arbitrary constants.

The incompressible approximation is normally taken to mean that density changes resulting from velocity changes may be ignored. However, in this case density changes due to the centrifugal pressure rise are also being ignored, which is a particularly bad approximation for compressors, in which pressure ratios of six or more are commonly achieved. The possibility of incorporating allowance for compressibility into the calculation method is discussed in Section 6.

The assumption that the flow is irrotational in the absolute frame of reference is in general incompatible with the quasi-two-dimensional approximation. Only when the blades are shaped so as to accept free-vortex flow can the two assumptions be made compatible. In the quasi-two-dimensional approximation the passage is divided into strips of which PQ in Fig. 3 is typical, and then the flow is taken to lie in these strips. However, if there is zero absolute rotation of the fluid then there must be relative rotation in the sense of the arrows in Fig. 3, which generally requires a radial component in the flow where the passage is axial. Radial flow is not accounted for in this approximation. Further along the impeller passage where the mean flow is nearly radial the relative rotation of the fluid plays a large part in determining the distribution of velocity. Ellis and Stanitz's [9] full calculation of a three-dimensional flow led them to conclude that the usual two-by-two dimensional method gave adequate results, particularly for the distribution of throughflow velocity over the blades. More recent work by Worster [10] questions this convenient conclusion. However, for investigating the changes produced by allowing a wake region to exist it seems reasonable to retain this approximation.

3 Flow Equations and Boundary Conditions

3.1 Coordinate System and Equations. It is usual to have a system of coordinates that are orthogonal and fixed either absolutely or relative to a moving impeller. Occasionally streamline coordinates are used, in which case they are generally used together with their normals, which for irrotational flow in a stationary system are the velocity potentials. In the present calculation the systems are mixed, with the relative streamlines as one coordinate and rotating meridional lines as the other coordinate; together these make up a nonorthogonal curvilinear system.

The equations governing the flow are those of continuity and absolute irrotational motion.

$$\frac{\partial u}{\partial m} + \frac{u}{r}\frac{dr}{dm} + \frac{u}{h}\frac{dh}{dm} + \frac{1}{r}\frac{\partial v}{\partial \theta} = 0 \qquad (1)$$

$$\frac{\partial v}{\partial m} + \frac{v}{r}\frac{dr}{dm} - \frac{1}{r}\frac{\partial u}{\partial \theta} + 2\Omega\frac{dr}{dm} = 0 \qquad (2)$$

These are made nondimensional in terms of r_2 the tip radius, h_2 the tip height and u_2 the mean radial velocity at the tip. In

Nomenclature

C = rotation number = $\dfrac{\Omega r_2}{u_2}$
h = passage height normal to mean flow surface
H = dimensionless height h/h_2
i, j = mesh counters in finite difference grid (Fig. 4)
m = meridional coordinate
M = dimensionless meridional coordinate = m/r_2
p = pressure
q = relative velocity
Q = dimensionless relative velocity = q/u_2
QR = ratio of velocity at separation to maximum velocity on blade surface
r = radius
R = dimensionless radius = r/r_2
u = meridional velocity
U = dimensionless meridional velocity u/u_2
v = relative tangential velocity
V = dimensionless tangential velocity = v/u_2
α = angle between blades in radians
$\Delta M, \Delta\psi$ = mesh lengths in M, ψ directions
θ = angular coordinate in radians relative to impeller
Θ = scaled angular coordinate = θ/α
ρ = density
ψ = stream function
Ω = angular velocity of impeller
Suffix 2 value at impeller tip

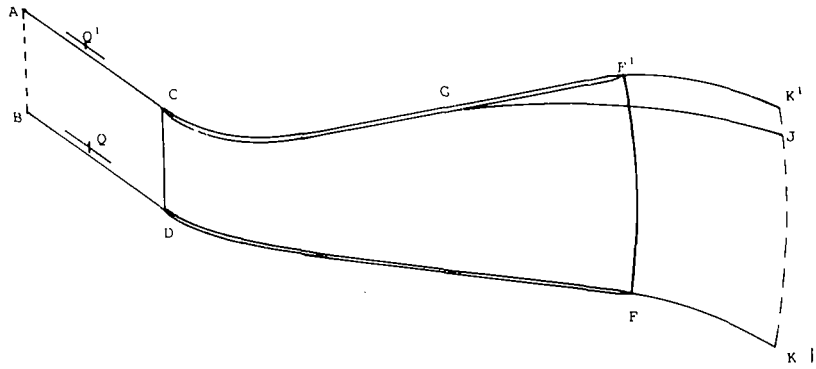

Fig. 2 Representation of an impeller passage

addition,

$$C = \frac{\Omega r_2}{u_2}$$

$$\Theta = \frac{\theta}{\alpha}$$

so that $\Theta = 0$ at the blade tip on the pressure side and $\Theta = 1$ at the blade tip on the suction side. Capital letters denote the dimensionless variables.

$$\frac{\partial U}{\partial M} + \frac{U}{R}\frac{dR}{dM} + \frac{U}{H}\frac{dH}{dM} + \frac{1}{R\alpha}\frac{\partial V}{\partial \Theta} = 0 \quad (3)$$

$$\frac{\partial V}{\partial M} + \frac{V}{R}\frac{dR}{dM} - \frac{1}{R\alpha}\frac{\partial U}{\partial \Theta} + 2C\frac{dR}{dM} = 0 \quad (4)$$

A stream function ψ is introduced, defined by the relations

$$U = \frac{1}{RH}\frac{\partial \psi}{\partial \Theta} \qquad V = \frac{-\alpha}{H}\frac{\partial \psi}{\partial M} \quad (5)$$

These relations satisfy equation (3) identically and also the conditions

$$\left.\begin{aligned} \psi = 1, \Theta = 1 \\ \psi = 0, \Theta = 0 \end{aligned}\right\} \text{ at } R = 1$$

Substitution into equation (4) leads to the stream function equation

$$\frac{\partial^2 \psi}{\partial M^2} + \frac{1}{R^2\alpha^2}\frac{\partial^2 \psi}{\partial \Theta^2} + \left(\frac{1}{R}\frac{dR}{dM} - \frac{1}{H}\frac{dH}{dM}\right)\frac{\partial \psi}{\partial M} - \frac{2CH}{\alpha}\frac{dR}{dM} = 0 \quad (6)$$

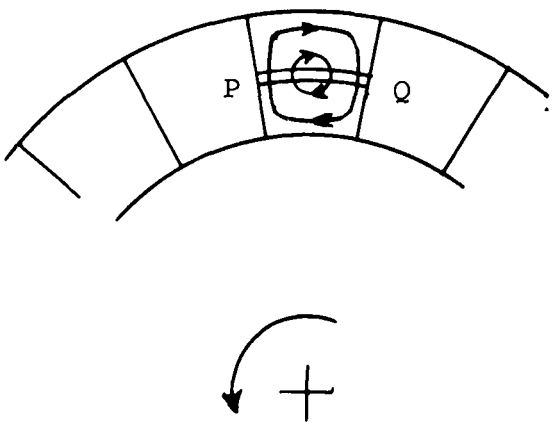

Fig. 3 Relative rotation at inlet to impeller passage

When equation (6) is solved by finite difference methods there are irregular mesh points on blade surfaces that are not radial. More important there must be irregular mesh points on the free shear layer which change as the calculation iteratively converges on the correct shape of interface. It is to escape from this difficulty that the equation is changed from the form

$$\psi(M, \Theta) = 0$$

to

$$\Theta(M, \psi) = 0$$

In the M, ψ system all the boundaries of the flow field are along lines either of constant M (far upstream and downstream) or of constant ψ (stagnation streamline upstream, blade surfaces, free shear layer and wake). This makes solution of the equation by a finite difference method much easier. The resulting equation is

$$\left(\frac{\partial \Theta}{\partial \psi}\right)^2 \frac{\partial^2 \Theta}{\partial M^2} - 2\frac{\partial \Theta}{\partial \psi}\frac{\partial \Theta}{\partial M}\frac{\partial^2 \Theta}{\partial \psi \partial M} + \left\{\left(\frac{\partial \Theta}{\partial M}\right)^2 + \frac{1}{R^2\alpha^2}\right\}\frac{\partial^2 \Theta}{\partial \psi^2} + \left(\frac{1}{R}\frac{dR}{dM} - \frac{1}{H}\frac{dH}{dM}\right)\frac{\partial \Theta}{\partial M}\left(\frac{\partial \Theta}{\partial \psi}\right)^2 + \frac{2CH}{\alpha}\frac{dR}{dM}\left(\frac{\partial \Theta}{\partial \psi}\right)^3 = 0 \quad (7)$$

The derivation of equation (7) from equation (6) is given in Appendix 2.

In the M, ψ system the stream function relations are

$$U = \frac{1}{RH\dfrac{\partial \Theta}{\partial \psi}} \qquad V = \frac{\alpha\dfrac{\partial \Theta}{\partial M}}{H\dfrac{\partial \Theta}{\partial \psi}} \quad (8)$$

3.2 Finite Difference Forms. Equation (7) is nonlinear, but when centered finite difference expressions for all the Θ derivations are inserted into the equation it becomes linear in the value of Θ at the center point. As an example the first term of equation (7) is written out in full with the notation of Fig. 4(*a*), using second order differences.

$$\left(\frac{\partial \Theta}{\partial \psi}\right)^2 \cdot \frac{\partial^2 \Theta}{\partial M^2} = \left(\frac{\Theta_{i,j+1} - \Theta_{i,j-1}}{2\Delta\psi}\right)^2 \cdot \left(\frac{\Theta_{i+1,j} - 2\Theta_{i,j} + \Theta_{i-1,j}}{(\Delta M)^2}\right)$$

$\Theta_{i,j}$ only appears once and so the expression is linear in $\Theta_{i,j}$. Since $\Theta_{i,j}$ only appears in the expressions for the second derivatives, and because second derivatives are not multiplied together anywhere in equation (7), the whole equation is linear in $\Theta_{i,j}$ when put into finite difference form.

The finite difference form of equation (7) is solved iteratively

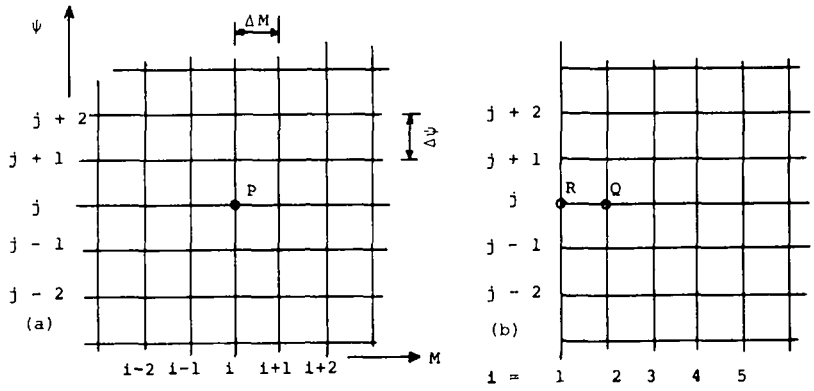

Fig. 4(a) Within the field
(b) By the boundary

at every internal mesh point. Instead of the second order finite difference expressions used in the example above, fourth order expressions are used for both first and second derivatives at every point that is not adjacent to a boundary, and third order expressions at every point that is adjacent to a boundary. For the cross derivative $\frac{\partial^2\Theta}{\partial\psi\partial M}$, which is small, a first order expression is used. These expressions are listed in Appendix 2.

When at other times in the calculation gradients are required, for example for evaluating velocities from equations (8), they are calculated from third order expressions, also listed in Appendix 2.

3.3 Boundary Conditions. (Sections of the boundary described below are shown on Fig. 2. The representation in Fig. 2 of the flow surface in one passage is described in Appendix 1).

Upstream. Along AB, a few mesh lengths upstream of the impeller, the flow is taken to be axisymmetric. Then $\frac{\partial\Theta}{\partial\psi} = 1$. Also the flux of angular momentum across AB, which is equal to the prewhirl, is specified. The transverse location of the boundary is then adjusted in every iteration to maintain this prewhirl.

Stagnation Streamlines. The streamline $\psi = 0$, BD, is the same as the streamline $\psi = 1$, AC, when it is regarded as belonging to the next impeller passage. Therefore values of Θ at points along either line may be calculated from Θ and ψ at points Q^1 being found by adding 1 to the values at Q.

Along the Blades. On the blades $\psi = 0$ or $\psi = 1$: Θ is given as a tabulated function of M.

Separation Point G. The flow is taken to separate from the suction side when the velocity has fallen to a specified fraction of the maximum velocity reached on that side of the passage. A more complicated criterion could be used if sufficient data to justify it were obtained. The flow is assumed to remain attached to the pressure side at all times.

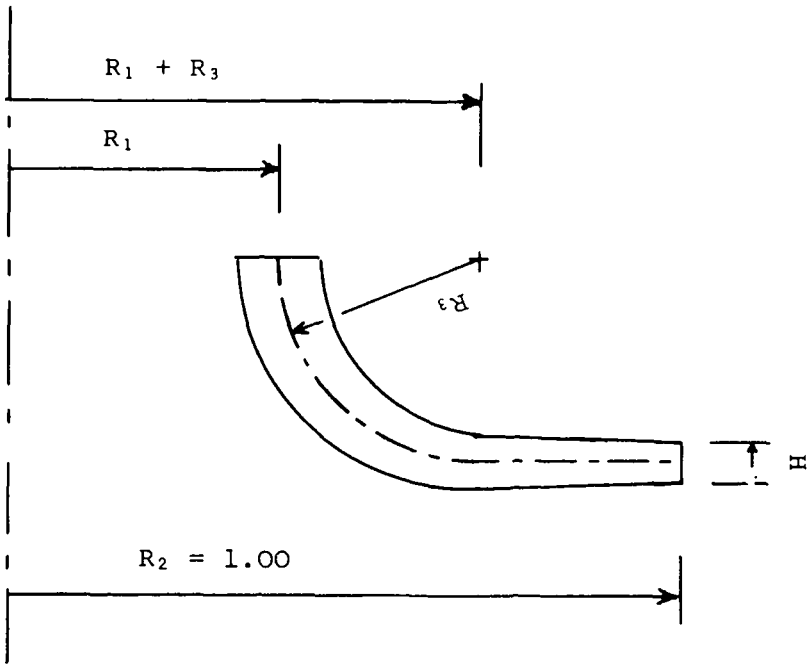

Fig. 5 Meridional view of impeller passage

Along the Free Shear Layer GJ. In the wake there is no flow, so there must be radial equilibrium.

$$\frac{dp}{dr} = \rho r\Omega^2$$

For incompressible flow

$$p = {}^1/_2\rho r^2\Omega^2 + \text{const.}$$

$(p - {}^1/_2\rho r^2\Omega^2)$ is therefore constant throughout the wake and along the shear layer. Along the shear layer, which is also a relative streamline, Euler's equation holds

$$dp + \rho q dq = \rho r\Omega^2 dr$$

$$p - {}^1/_2\rho r^2\Omega^2 = -{}^1/_2\rho q^2 + \text{const.}$$

So along the shear layer ${}^1/_2\rho q^2$ and therefore Q are constant. From equation (8)

$$Q^2 = U^2 + V^2$$

$$= \frac{\alpha^2}{H^2\left(\frac{\partial\Theta}{\partial\psi}\right)^2}\left\{\frac{1}{R^2\alpha^2} + \left(\frac{\partial\Theta}{\partial M}\right)^2\right\} \qquad (9)$$

$$= \text{the value of } Q^2 \text{ at separation.}$$

The finite difference form of equation (9) is solved iteratively at points along the shear layer to find its position.

Along the Shear Layer FK. From the influence of the Coriolis acceleration on stability one would expect to find that mixing was intensified on this shear layer, and that the liquid surface analogy was therefore particularly inappropriate. However, the assumption made here is the same as that for the shear layer GJ. This is mainly for simplicity, because an error in the prediction of the flow in this region is unlikely to have much influence on

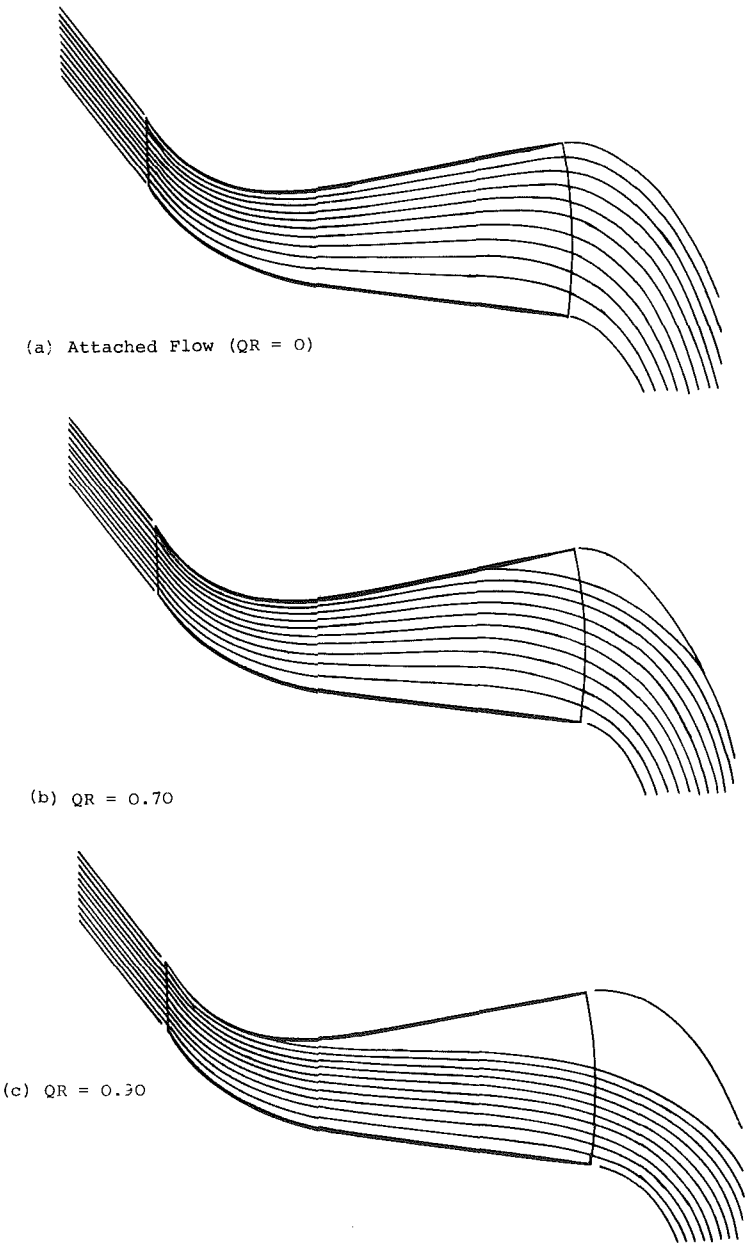

Fig. 6 Relative streamlines in radial-tipped impeller at C = 3.0

the flow in the impeller passage itself. However, the streamline FK may be so sharply curved that it is in fact stabilized. Such unexpected stabilization of the shear layer leaving the pressure surface has been demonstrated experimentally by Senoo and Ishida (13), but the corresponding region of GJ is then destabilized.

Across the Outlet. At the downstream boundary the flow may either be still divided into a jet and a wake as in Figs. 2 and 6(*c*), or the wake may have closed up as in Fig. 6(*b*). In the first case the flow across JK is taken to be uniform and at the same velocity as on the shear layers. In the second case the flow is taken to be axisymmetric with $\frac{\partial \Theta}{\partial \psi} = 1$.

In either case the transverse location of the downstream boundary is adjusted in each iteration to insure that the flow leaves the impeller smoothly in the direction of the trailing edge.

3.4 Torque and Flux of Angular Momentum. The torque on the impeller is calculated by integration of the pressure difference across a passage along the length of the passage. Comparison of this quantity with the change in flux of absolute angular momentum from inlet to outlet serves as an additional check on the method.

The flux of absolute angular momentum across an arc is useful for estimation of the upstream whirl and the slip factor. It is also useful as a check on the accuracy of the numerical method, since it should not vary with radius downstream of the impeller.

The expression for the flux is

$$\int_0^1 R\alpha(V + CR)d\psi$$

$$= R^2C\alpha + R\alpha\int_0^1 Vd\psi$$

Integration is by Simpson's rule.

4 Preliminary Results

4.1 Attached Flow. A test of the calculation method is to compare its predictions for a fully attached flow with those of Stanitz [1]. In Stanitz's example the positions of the streamlines were calculated for $R > 0.675$, with the assumption that at that radius neither the inlet nor the outlet influenced the flow, so that the flow direction was purely radial while at the same time the flow was still irrotational. For the comparison, where the flow in an entire impeller passage is calculated, an impeller was chosen with an arbitrary but convenient shape for $R < 0.675$. In this impeller the blades were thin, straight and radial from $R = 0.60$ outwards, and the shape of the passage in the meridional plane was as shown in Fig. 5, with $R_1 = 0.35$, $R_3 = 0.25$, and $H = 1/R$ throughout the impeller and also in the vaneless diffuser. The blade inlet angle of 45 deg gave approximately zero incidence at $C = 3.0$, the value chosen by Stanitz.

The streamline patterns obtained with the two calculation methods are shown superposed in Fig. 7. The differences between the two are discussed in Section 5.1.

4.2 Separated Flows. The cases calculated with separated flow fall into two groups, those in which the velocity ratio to separation was varied and those in which the rotation number (or throughflow) was varied.

For a radial-tipped impeller the flow pattern was calculated at six values of QR; 0.0 (attached flow), 0.60, 0.70, 0.80, 0.90 and 0.99. From the solutions at QR = 0.0, 0.70 and 0.90 the streamline patterns are reproduced in Fig. 6 and the blade velocities plotted in Fig. 8. The variation of the slip factor with QR is plotted in Fig. 9.

In both radial tipped and backward curved impellers flow patterns were calculated with varying rotation number for both separated and attached flow. The variations in slip factor are plotted in Fig. 10. Streamline patterns for separated flow in a backward curved impeller at three different rotation numbers are reproduced in Fig. 11.

The coordinate transformation for plotting the streamlines is described in Appendix 1.

4.3 Impeller Shapes. Just two impeller shapes were used for all the calculations except the comparison with Stanitz's results. The radial-tipped impeller is shown in the meridional view in Fig. 5, with $R_1 = 0.40$ and $R_3 = 0.30$. The inlet angle was 60 deg, and the blades were straight and radial from $R = 0.70$ outwards. The blade thickness was 2 percent of the passage width, tapering to zero at inlet and outlet. The passage height H varied inversely as the square root of the meridional coordinate M, where $M = 1$ at the tip, an arrangement which gave an area ratio of approximately 1:2.2. There were twenty blades. The vaneless diffuser was of constant depth.

The backward-curved impeller was identical except that the blades were curved back from being radial at $R = 0.70$ to an angle of 30 deg to the radius at the tip.

5 Discussion of Results

5.1 Comparison With Stanitz. The comparison in Fig. 7 be-

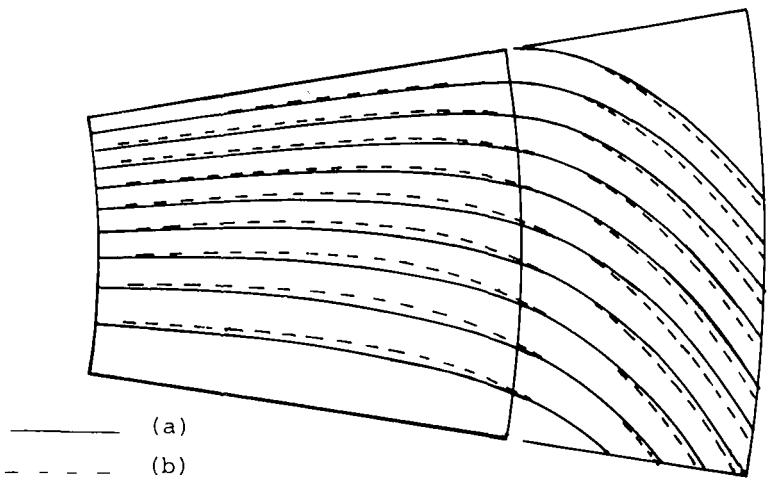

Fig. 7 Relative streamlines in attached flow
(*a*) From present calculation method
(*b*) From Stanitz (Reference [1])

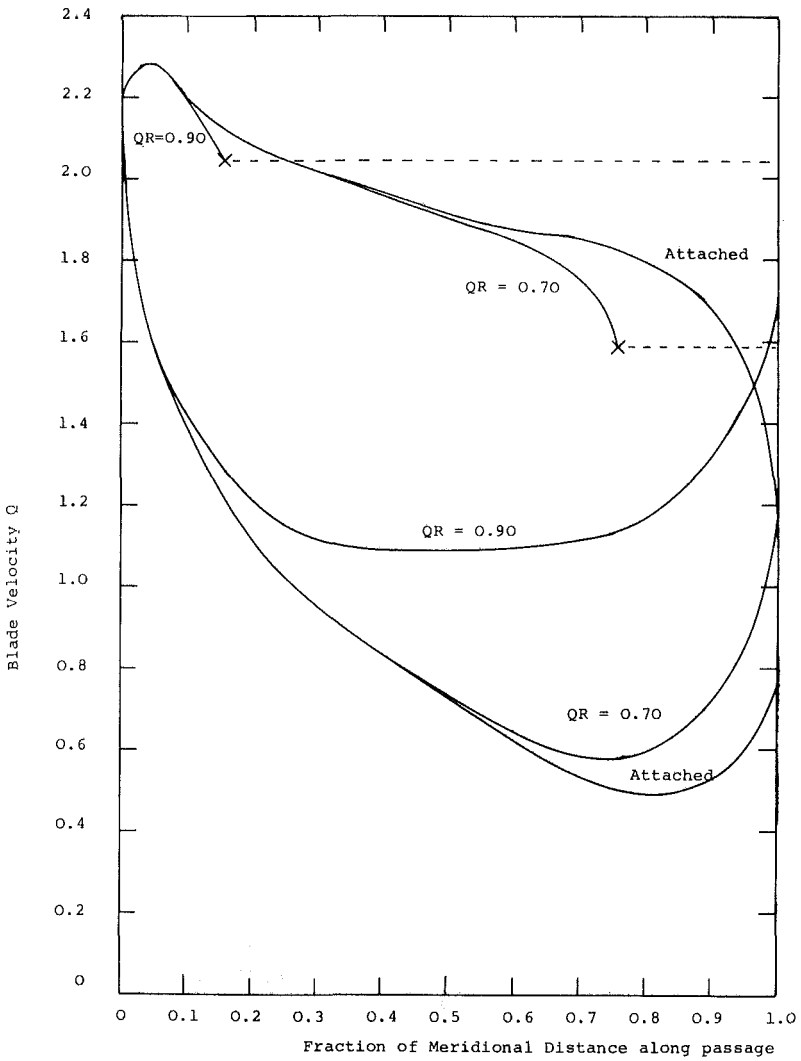

Fig. 8 Blade velocities in radial-tipped impeller at $C = 3.0$

tween an attached flow calculated with the present method and one calculated by Stanitz [1] shows a slight difference in the streamline patterns. The effect of the difference in the directions of the streamlines at the impeller tip is that whereas Stanitz predicted a slip factor of 0.892 the present method predicts one of 0.92. Whether the difference between these figures is due to

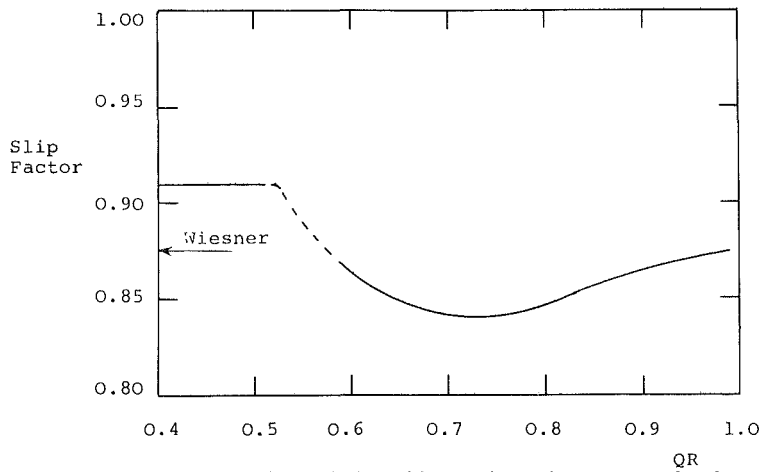

Fig. 9 Variation of slip factor with velocity ratio to separation in radial-tipped impeller at $C = 3.0$

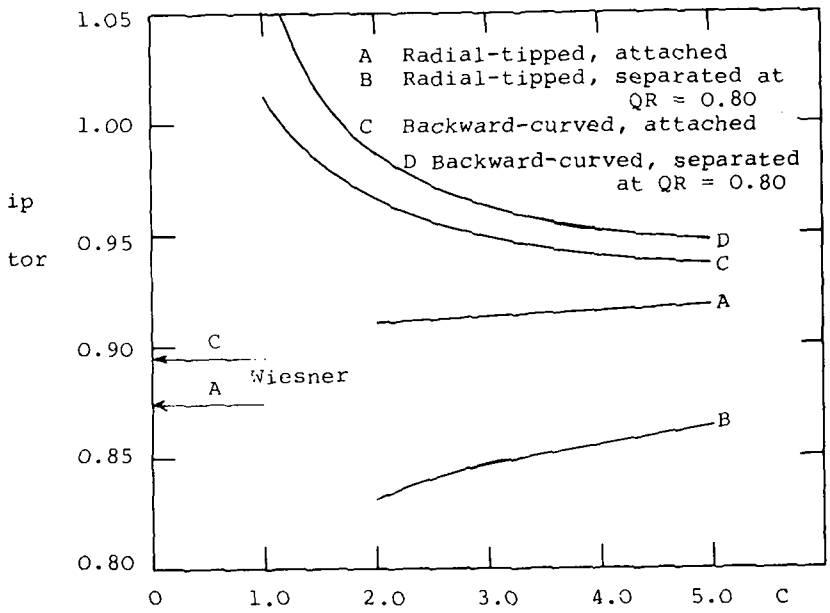

Fig. 10 Variation of slip factor with rotation number

coarseness of the finite difference mesh or a more fundamental cause has not yet been determined. Downstream of the impeller the flux of absolute angular momentum should not vary; however, a variation of 1.2 percent is found in the calculation here.

Although the agreement between the streamline patterns produced by the two methods is fairly good in this example, it would not be so at a higher rotation number. In the finite difference form of equation (7) in Section 3.1, Θ must remain a single-valued function of ψ, with the result that a recirculation bubble of the type calculated by Stanitz at high rotation number (low flow) would not be predicted. This is a minor drawback to the calculation method as such recirculation is not found in real impellers.

5.2 Velocity Ratio to Separation. The choice of the ratio of the velocity at separation to the highest velocity attained on the suction side is at this stage arbitrary. Values quoted range from about 0.4 for turbulent to about 0.95 for laminar boundary layers in stationary systems, and it is likely that in the present case of a turbulent layer with suppressed mixing the best value will be between these two figures.

The velocity distribution over the blade surfaces plotted in Fig. 8 shows that there is a large reduction in velocity over the last part of the blade when the flow is attached. If this actually occurred there would be a corresponding large pressure gradient in this region which would probably lead to separation. When there is separation the modification of the rest of the flow field leads to an adverse pressure gradient in the last part of the flow before it separates, which means that specification of a maximum adverse velocity gradient would be an unsuitable criterion for determining the position of the separation point.

From the streamline patterns of Fig. 6 it can readily be seen how for a higher ratio the separation is earlier, the width of the wake is greater and the wake penetrates further downstream into the diffuser before closing up. In this example the ratio of the tip velocity to the highest velocity on the suction side is about 0.53 when the flow is attached, so specification of a lower ratio to separation would lead to prediction of attached flow.

5.3 Slip Factor. The slip factor is important since it is proportional to the work input to the impeller. It is therefore useful to be able to predict it accurately. As the velocity ratio to separation is increased Fig. 9 shows how first the slip factor decreases as the suction surface loses its guiding influence on the flow, and then increases again as the flow becomes more like a jet following the pressure surface.

Most correlation methods for predicting slip factor, such as those discussed by Wiesner [12], take no account of any variation with flow rate. Indeed Stanitz [2] in his calculations on a radial-tipped impeller found no significant variation. However, Fischer and Thoma [5] observed that the flow followed the blades of a backward-curved impeller more closely, and therefore the slip factor increased, as the throughflow was reduced. Also Johnston and Dean [13] in Fig. 11 of their paper showed that for a radial-tipped impeller the slip factor rose from 0.8 to 1.0 as the rotation number (the inverse of a flow coefficient) was raised from 2.0 to 6.5.

Fig. 10 shows the variation of slip factor with rotation number for four cases, i.e., radial and backward curved impellers, each with attached flow and flow that separated at a velocity ratio of 0.80. In curve A, for attached flow past radial blades, the small variation of less than 1 percent agrees with the findings of Stanitz [2]. In curve B for separated flow there is a reduction of the slip factor to values nearer those of about 0.87 tabulated by Wiesner [12] from measurements on impellers. The increase of slip factor as the rotation number is raised from 2.0 to 5.0 is in the correct sense, but still not large.

In curves C and D for backward curved blades the variation of slip factor with rotation number is in the opposite direction to that found with radial blades. This can be explained by the way in which the blades do less work on the fluid as the flow rate is increased, until at $C = 1.0$ the fluid is doing work on the blades over the last part of the impeller passage, leading to a slip factor greater than 1.0. The streamline pattern for this case is shown in Fig. 11(*c*). The situation described by Fischer and Thoma [5], where the flow becomes a thin jet along the pressure surface, leading to an increased slip factor, was not reached because the area ratio of the impeller was not large enough.

For comparison the slip factor of Wiesner's formula is marked on Figs. 9 and 10. For the type of impeller considered here the value of Busemann's slip factor is almost identical, according to the graphical comparison of the two slip factors presented by Wiesner [12].

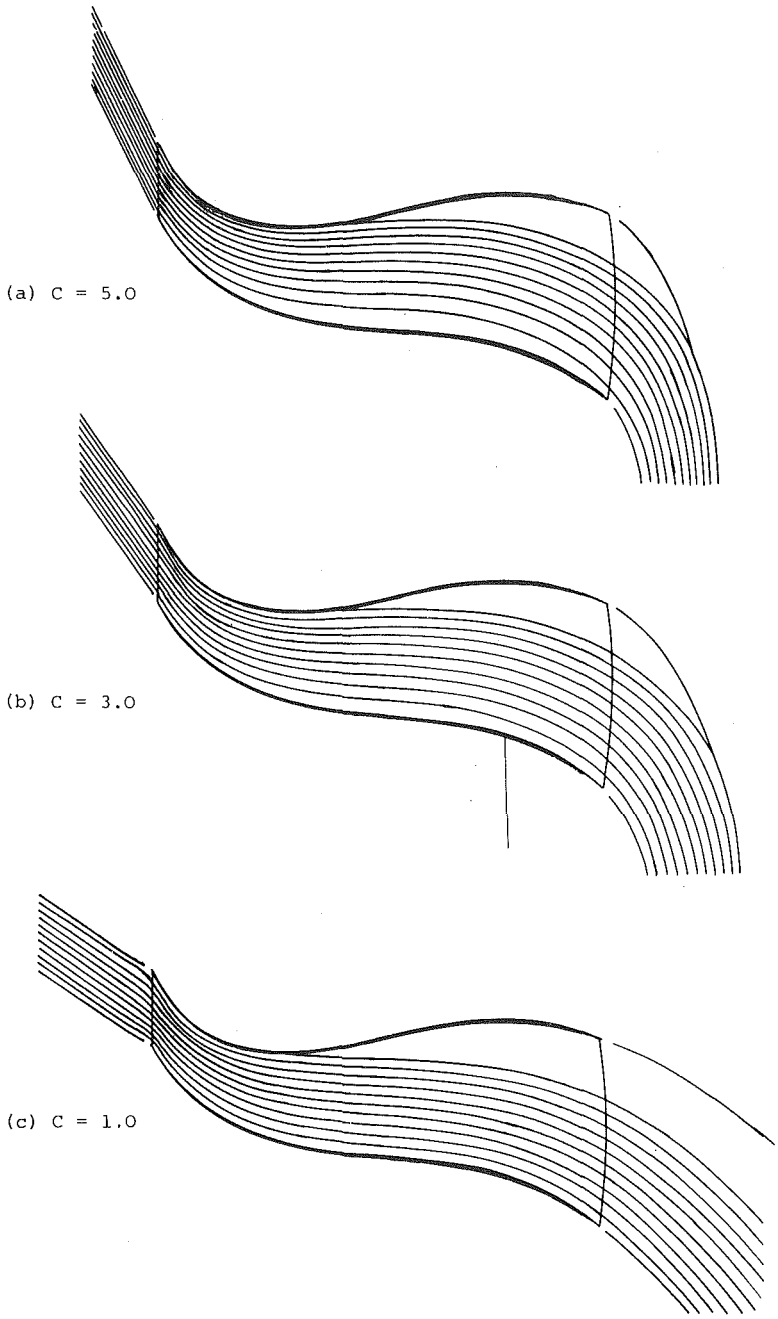

Fig. 11 Relative streamlines in backward-curved impeller with separation at QR = 0.80

5.4 Effect of Varying Throughflow on the Wake. Fig. 11 shows the streamline patterns in the backward-curved impeller at three different rotation numbers. As the rotation number is reduced from 5.0 to 1.0 (the throughflow is increased) the separation point moves very little and the width of the wake at the tip is almost unchanged. However, the distance that the wake penetrates downstream into the diffuser is greatly increased. Johnston and Dean [13] considering a jet and a wake entering a diffuser predict a much more rapid closing up of the wake, but the trend is in the same direction.

6 Extension to Compressible Flow

The system of inversion of the stream function equation described in Section 3.1 is applicable to compressible flow just as to incompressible flow, but the addition of the density as another variable further complicates the equations.

The compressible form of equation (7) contains the density and density gradients. The equation defining the compressible stream function relates the relative velocity to the density and the steam function gradients. A third equation derived from the steady flow energy equation and the perfect gas laws relates the same variables, so from these three equations there is enough information to solve for both the streamline pattern and the density distribution.

On the free shear layer the boundary condition is more complicated than before. Now the absolute static pressure variation along the streamline bounding the flow must match the abiabatic centrifugal pressure rise in the wake. From this condition an equation for the density distribution along the shear layer may be obtained, and from this the velocity distribution.

7 Conclusions

7.1 With the jet and wake calculation method described in this report it has been shown how the streamline pattern and the overall parameters for the flow in a centrifugal impeller are changed by altering the flow rate, the ability of the suction side boundary layer to withstand diffusion, or the impeller shape. The few results presented here are merely examples of the types of variations that can be studied.

The magnitude of the slip factor predicted with the separated flow calculation for a radial-discharge impeller was nearer to that found in machines than the higher figures predicted with attached flow, and the variation with flow rate was in the right direction. In a backward curved impeller the effect of separation on the slip factor was smaller and in the opposite direction.

7.2 Further Work. The incompressible flow model should now be applied to some actual impeller designs to see how its predictions compare with observations.

The effects of compressibility should be incorporated into the calculation method so that it can be used to predict the flow in a high pressure ratio impeller, for comparison with experimental results.

An experimental program is in progress in which the incompressible flow in a single rotating rectangular channel is being studied. In this work a criterion for separation of the flow from the suction side is being sought, either of the velocity ratio type used in the present calculation method or perhaps a limit of the velocity gradient along the wall before separation occurs.

References

1 Stanitz, J. D., "Two-dimensional Compressible Flow in Turbomachines with Conic Flow Surfaces," N.A.C.A. Report 935, 1952.

2 Stanitz, J. D., "Some Theoretical Aerodynamic Investigations of Impellers in Radial and Mixed-Flow Centrifugal Compressors," *Trans. A.S.M.E.*, Vol. 74, 1952, p. 473.

3 Katsanis, Th., "Use of Arbitrary Quasi-orthogonals for Calculating Flow Distribution in a Turbomachine," *Trans. A.S.M.E. Journal of Engineering for Power*, Vol. 88, 1966, p. 197.

4 Senoo, Ya., and Nakase, Yo., "A Blade Theory of an Impeller with an Arbitrary Surface of Revolution," *Trans. A.S.M.E. Journal of Engineering for Power*, Vol. 93, 1971, p. 454.

5 Fischer, K., and Thoma, D., "Investigation of the Flow Conditions in a Centrifugal Pump," *Trans. A.S.M.E.*, Paper No. HYD-54-8, 1932.

6 Dean, R. C., "Advanced Radial Compressors," von Karman Institute, Lecture Series 50, 1972.

7 Dean, R. C., "The Fluid Dynamic Design of Advanced Centrifugal Compressors," Lecture Notes, Creare TN-180, 1973.

8 Bradshaw, P., "Effects of Streamline Curvature on Turbulent Flow," NATO AGARD No. 169, 1973.

9 Ellis, G. O., and Stanitz, J. D., "Comparison of Two and Three-dimensional Potential Flow—Solutions in a Rotating Impeller Passage," N.A.C.A. TN 2806, 1952.

10 Worster, D. M., "The Calculation of Fully Three-Dimensional Flows in Impellers Using a Finite Element Method," Report from Department of Mechanical Engineering at Heriot-Watt University, Edinburgh, 1973.

11 Senoo, Ya., and Ishida, M., "Behaviour of Severely Asymmetric Flow in a Vaneless Diffuser," A.S.M.E. Paper No. 74-GT-64, 1974.

12 Wiesner, F. J., "A Review of Slip Factors for Centrifugal Impellers," *A.S.M.E. Journal of Engineering for Power*, Vol. 89, 1967, p. 558.

13 Johnston, J. P., and Dean, R. C., "Losses in Vaneless Diffusers of Centrifugal Compressors and Pumps," *A.S.M.E. Journal of Engineering for Power*, Vol. 88, 1966, p. 49.

14 Halleen, R. M., and Johnston, J. P., "The Influence of Rotation on Flow in a Long Rectangular Channel—An Experimental Study," Stanford University, Department of Mechanical Engineering, Report MD-18, 1967.

15 Lezius, D. K., and Johnston, J. P., "The Structure and Stability of Turbulent Wall Layers in Rotating Channel Flow," Stanford University, Department of Mechanical Engineering, Report MD-29, 1971.

APPENDIX 1

Representation of the Impeller Passage

The mean flow surface in an impeller passage cannot be developed into a flat surface without distortion. Therefore a method has been found to present the flow surface in a diagram such as those of Figs. 2, 6, 7 and 11. The transformation described here is acceptable only if the angle between the blades is not large.

The transformation is

$$X = M - \frac{R}{\frac{dR}{dM}}\left\{1 - \cos\left[(\theta - \theta_0)\frac{dR}{dM}\right]\right\}$$

$$Y = \frac{R}{\frac{dR}{dM}}\sin\left[(\theta - \theta_0)\frac{dR}{dM}\right]$$

where θ_0 is chosen to keep the distortion small. In the axial inlet region these reduce to

$$X = M$$

$$Y = R(\theta - \theta_0)$$

which represents a true development of the cylindrical flow surface. In the radial outlet region they reduce to

$$X = R\cos(\theta - \theta_0)$$

$$Y = R\sin(\theta - \theta_0)$$

which represents the radial plane in a true view. In the mixed flow region there is distortion of the flow surface, which is only slight for a twenty-bladed impeller.

APPENDIX 2

Inversion of Stream Function Equation and List of Finite Difference Expressions

2a Derivation of Equation (7) from Equation (6). In this section the notation $\left.\frac{\partial\psi}{\partial\Theta}\right|_M$ is used to mean the rate of change of ψ with Θ at constant M.

The first necessary relation is

$$\left.\frac{\partial\psi}{\partial\Theta}\right|_M = \frac{1}{\left.\frac{\partial\Theta}{\partial\psi}\right|_M} \tag{A}$$

From the identity

$$\left.\frac{\partial\psi}{\partial\Theta}\right|_M \cdot \left.\frac{\partial\Theta}{\partial M}\right|_\psi \cdot \left.\frac{\partial M}{\partial\psi}\right|_\Theta = -1$$

$$\left.\frac{\partial\psi}{\partial M}\right|_\Theta = \frac{\left.\frac{\partial\Theta}{\partial M}\right|_\psi}{\left.\frac{\partial\Theta}{\partial\psi}\right|_M} \tag{B}$$

These relations substituted into equations (5) lead to equations (8) for the velocities in terms of the other variables.

Manipulation of the identity

$$dF = \left.\frac{\partial F}{\partial M}\right|_\Theta dM + \left.\frac{\partial F}{\partial\Theta}\right|_M d\Theta = \left.\frac{\partial F}{\partial M}\right|_\psi dM + \left.\frac{\partial F}{\partial\psi}\right|_M d\psi \tag{C}$$

where F is any dependent variable leads to

$$\left.\frac{\partial^2\psi}{\partial M^2}\right|_\Theta = -\frac{\left.\frac{\partial\Theta}{\partial\psi}\right|_M^2 \left.\frac{\partial^2\Theta}{\partial M^2}\right|_\psi + 2\left.\frac{\partial\Theta}{\partial\psi}\right|_M \left.\frac{\partial\Theta}{\partial M}\right|_\psi \frac{\partial^2\Theta}{\partial\psi\partial M} - \left(\left.\frac{\partial\Theta}{\partial M}\right|_\psi\right)^2 \left.\frac{\partial^2\Theta}{\partial\psi^2}\right|_M}{\left(\left.\frac{\partial\Theta}{\partial\psi}\right|_M\right)^3} \tag{D}$$

and

$$\left.\frac{\partial^2\psi}{\partial\Theta^2}\right|_M = \frac{-\left.\frac{\partial^2\Theta}{\partial\psi^2}\right|_M}{\left(\left.\frac{\partial\Theta}{\partial\psi}\right|_M\right)^3} \tag{E}$$

Relations (B), (D) and (E) are substituted into equation (6) to obtain equation (7).

2b Finite Difference Expressions. For points that are not adjacent to a boundary such as P in Fig. 4(a), the following fourth order finite difference expressions for the derivatives are used.

$$\frac{\partial\Theta}{\partial M} = \frac{-\Theta_{i+2,j} + 8\Theta_{i+1,j} - 8\Theta_{i-1,j} + \Theta_{i+2,j}}{12\Delta M}$$

$$\frac{\partial^2\Theta}{\partial M^2} = \frac{-\Theta_{i+2,j} + 16\Theta_{i+1,j} - 30\Theta_{i,j} + 16\Theta_{i-1,j} - \Theta_{i-2,j}}{12(\Delta M)^2}$$

with similar expressions for $\frac{\partial\Theta}{\partial\psi}$ and $\frac{\partial^2\Theta}{\partial\psi^2}$.

For points that are adjacent to a boundary, such as Q in Fig. 4(b), these third order expressions are used.

$$\frac{\partial\Theta}{\partial M} = \frac{-2\Theta_{1,j} - 3\Theta_{2,j} + 6\Theta_{3,j} - \Theta_{4,j}}{6\Delta M}$$

$$\frac{\partial^2\Theta}{\partial M^2} = \frac{\Theta_{1,j} - 2\Theta_{2,j} + \Theta_{3,j}}{(\Delta M)^2}$$

At all points the following first order expression is used for the cross derivative, which is small everywhere except close to the leading edge when there is incidence.

$$\frac{\partial^2\Theta}{\partial\psi\partial M} = \frac{\Theta_{i+1,j+1} - \Theta_{i-1,j+1} + \Theta_{i-1,j-1} - \Theta_{i+1,j-1}}{4\Delta\psi \cdot \Delta M}$$

For calculation of a gradient normal to a boundary, such as at R in Fig. 4(b), which is needed to obtain the velocity on a balde surface, this third order expression is used.

$$\frac{\partial\Theta}{\partial M} = \frac{2\Theta_{4,j} - 9\Theta_{3,j} + 18\Theta_{2,j} - 11\Theta_{1,j}}{6\Delta M}$$

All the expressions listed above are derived from polynomial approximations to the function $\Theta(M, \psi)$.